RSC Advances

PAPER

View Article Online
View Journal | View Issue

Cite this: *RSC Adv.*, 2018, **8**, 18400

Impact of bulky phenylalkyl substituents on the air-stable n-channel transistors of birhodanine analogues†

Kodai Iijima,[a] Yann Le Gal,[b] Dominique Lorcy[b] and Takehiko Mori*[a]

Received 19th April 2018
Accepted 11th May 2018

DOI: 10.1039/c8ra03362e

rsc.li/rsc-advances

By introducing bulky 2-phenylethyl groups into sulfur-rich electron acceptors, 5,5′-bithiazolidinylidene-2,2′-dione-4,4′-dithione and 5,5′-bithiazolidinylidene-2,4,2′,4′-tetrathione, electron transport with the mobility of 0.27 $cm^2 V^{-1} s^{-1}$ with ambient and long-term stability is achieved in thin-film transistors. Bulky groups destroy the intermolecular S–S network, but the long-term transistor stability is maintained. Here, benzyl groups realize one-dimensional stacking structures, whereas 2-phenylethyl groups lead to herringbone structures.

Introduction

Recent progress in organic transistors have achieved as high mobility as amorphous silicon and oxide semiconductors in the hole-transporting (p-type) materials.[1] Electron transporting (n-type) transistors, however, still have lots of room for improvement, particularly from the viewpoint of ambient stability.[2] Such n-type molecules as naphthalene diimides, perylene diimides, quinoidal oligothiophenes, and fluorinated acenes have been investigated, in which diimide compounds are suitable for not only small-molecule semiconductors but also components of polymer units. Diketopyrrolopyrrole, isoindigo, benzothiadiazole, and naphtobisthiadiazole are also useful as acceptor units in polymer n-type semiconductors.

Previously, we have reported remarkable transistor characteristics and air stability in n-type organic transistors of sulfur-rich acceptors, 3,3′-dialkyl-5,5′-bithiazolidinylidene-2,2′-dione-4,4′-dithione (**OS-R**) and 3,3′-dialkyl-5,5′-bithiazolidinylidene-2,4,2′,4′-tetrathiones (**SS-R**) (R = alkyl in Scheme 1).[3,4] **SS-R** compounds show stronger electron acceptor ability than **OS-R** stemming from the stability of the thiolate units (S^-) because the negative charges are largely located on the inner thiocarbonyl groups. **SS-Pr** shows the highest mobility of 0.26 $cm^2 V^{-1} s^{-1}$ among this series of materials, and achieves remarkable long-term stability even in the thin-film transistors. **SS-R** compounds form stacks with anisotropic two-dimensional carrier pathways. On the other hand, **OS-R** derivatives, which are easily available in a one-step reaction,[5] are organized into herringbone structures. These different molecular packings are attributed to the reduced S–S intermolecular interactions in **OS-R**. **OS-Et** thin-film transistors exhibit similar performance to **SS-Pr**. This is likely to come from the isotropic two-dimensional carrier pathways in the herringbone packing.[6] Transistors of **SS-R** maintain the performance for months, but **OS-R** transistors show slight degradation in air. Although **SS-R** is a stronger acceptor than **OS-R**, the excellent air stability has been ascribed to the extensive intermolecular S–S network in the **SS-R** compounds.[3,4]

We have reported that performance of transistors based on indigo is remarkably improved by the phenyl substitution.[7] Similar enhancement has been achieved thanks to the presence of phenyl rings in thienoisoindigo series.[8] In both cases, the improved performance is ascribed to the brickwork structure of the core parts as well as the herringbone arrangement of the phenyl rings. Note also that the presence of bulky substituents is not crippling; in p-type transistors based on TTF derivatives, *tert*-butyl substitution of hexamethylenetetrathiafulvalene (HMTTF) and dibenzo-TTF (DBTTF), improves the transistor

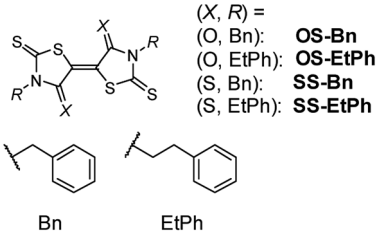

Scheme 1 Molecular structures, where R = benzyl (Bn) and 2-phenylethyl (EtPh). Compounds with X = O and S are respectively abbreviated as OS-R and SS-R.

[a]*Department of Materials Science and Engineering, Tokyo Institute of Technology, O-okayama 2-12-1, Meguro-ku, 152-8552, Japan. E-mail: mori.t.ae@m.titech.ac.jp*

[b]*Univ. Rennes, CNRS, ISCR (Institut des Sciences Chimiques de Rennes) - UMR 6226, F-35000 Rennes, France*

† Electronic supplementary information (ESI) available: Additional information for preparative details, devices fabrication, transistor characteristics, crystal structures. CCDC 1835173–1835176. For ESI and crystallographic data in CIF or other electronic format see DOI: 10.1039/c8ra03362e

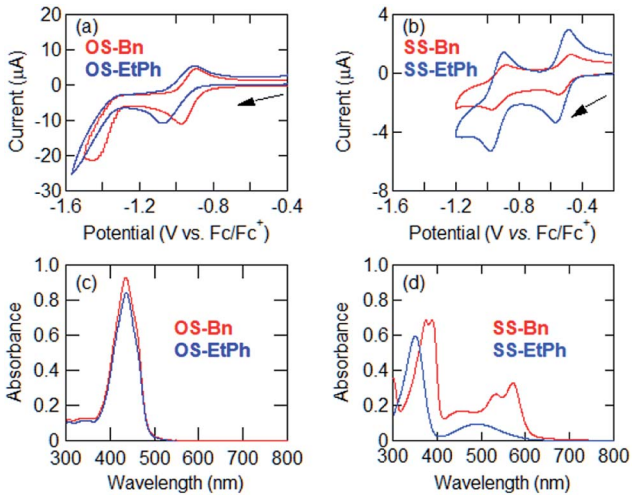

Fig. 1 Cyclic voltammograms of (a) OS-R and (b) SS-R. Absorption spectra of (c) OS-R and (d) SS-R.

properties due to closely packed organization.[9] In the present work, we demonstrate the influence of phenylalkyl substitutions of **OS-R** and **SS-R** (Scheme 1). We can expect that such bulky substituents improve the performance and stability of the transistors.

Results and discussion

Synthesis and electronic properties

SS-Bn and **SS-EtPh** were prepared in a similar manner as described in ref. 10. The one-step reaction was used for the synthesis of **OS-Bn** and **OS-EtPh** in the presence of triethylamine to complete the reaction.[5] We found that the addition of triethylamine was important, otherwise the central double bond remained hydrogenated.

The energy levels are estimated using cyclic voltammetry by measuring the redox potentials. In **SS-Bn** and **SS-EtPh**, the cyclic voltammograms clearly show two reversible reduction waves, while **OS-Bn** and **OS-EtPh** show only a single reversible reduction wave (Fig. 1(a) and (b)). The first half-wave potentials afford the lowest unoccupied molecular orbital (LUMO) levels (E_{LUMO}) as shown in Table 1. The LUMO levels of **SS-Bn** and **SS-EtPh** are −4.29 and −4.28 eV, respectively. These values are approximately equal to the previous **SS-R**,[4] indicating that the presence of the *N*-phenyl alkyl substituents do not significantly modify the electron accepting ability. Therefore, these derivatives are promising candidates to afford air-stable n-type transistor characteristics.[12] The LUMO levels of **OS-Bn** and **OS-EtPh** are situated above −4.0 eV, as previously observed for other **OS-R** derivatives.[4]

The energy gaps are extracted from the ultraviolet-visible spectra (Fig. 1(c) and (d)). **OS-Bn** and **OS-EtPh** show larger gaps (2.6 eV) than those of **SS-Bn** and **SS-EtPh** (2.0 eV). The highest occupied molecular orbital (HOMO) levels are estimated by subtracting the optical gaps from the LUMO levels. The HOMO levels are located at approximately the same levels in **OS-R** and **SS-R** (Table 1).

Transistor characteristics

Bottom-gate top-contact thin-film transistors were fabricated by vacuum evaporation of **OS-R** and **SS-R** on a SiO_2/Si substrate (300 nm SiO_2) treated with tetratetracontane (TTC).[13] Gold was used as source and drain electrodes. The transistor properties were measured under vacuum and in air (Table 2).

Thin-film transistors of **SS-Bn** does not work even under vacuum. All the other transistors exhibit n-type transistor

Table 1 Redox potentials, energy levels, and optical gaps of the acceptors[a]

	$E_1^{1/2}$ (V *vs.* Fc/Fc$^+$)	$E_2^{1/2}$ (V *vs.* Fc/Fc$^+$)	LUMO (eV)	λ_{edge} (nm)	Optical gap (eV)	HOMO (eV)
OS-Bn	−0.94	—	−3.86	485	2.56	−6.42
OS-EtPh	−0.99	—	−3.81	483	2.57	−6.38
SS-Bn	−0.51	−0.94	−4.29	608	2.04	−6.33
SS-EtPh	−0.52	−0.93	−4.28	607	2.04	−6.32

[a] The LUMO levels were estimated by assuming the reference energy level of ferrocene/ferrocenium to be 4.8 eV from the vacuum level.[11] The HOMO levels were obtained from the LUMO levels and the optical gaps.

Table 2 Transistor characteristics of the thin-film transistors

	After storage	Measurement	μ_{max} (cm^2 V^{-1} s^{-1})	$\mu_{average}$ (cm^2 V^{-1} s^{-1})	V_{th} (V)	On/off ratio
OS-Bn		Under vacuum	7.2×10^{-3}	6.7×10^{-3}	11	5×10^5
		In air	8.1×10^{-3}	6.8×10^{-3}	41	4×10^4
OS-EtPh		Under vacuum	2.0×10^{-2}	1.5×10^{-2}	24	8×10^5
		In air	1.4×10^{-2}	1.1×10^{-2}	52	6×10^5
SS-EtPh		Under vacuum	0.18	0.13	26	1×10^7
		In air	0.27	0.14	20	9×10^6
	Three months in air	Under vacuum	0.19	0.17	60	2×10^7
		In air	0.20	0.17	55	2×10^7

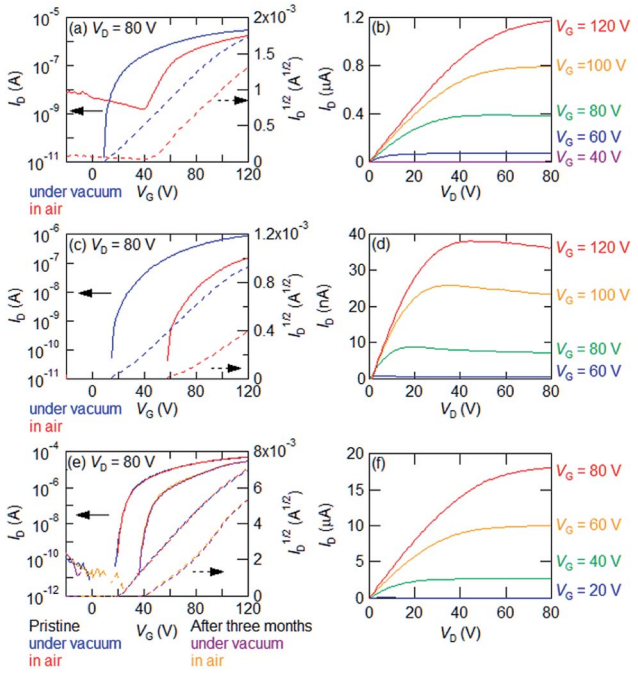

Fig. 2 (a) Transfer, and (b) output characteristics of **OS-Bn** thin-film transistors. (c) Transfer, and (d) output characteristics of **OS-EtPh** thin-film transistors. (e) Transfer, and (f) output characteristics of **SS-EtPh** thin-film transistors measured under vacuum (blue) and in air (red) just after the fabrication, together with the results after three-month storage in air, measured under vacuum (purple) and in air (yellow).

characteristics (Table 2). Transfer characteristics of an **SS-EtPh** thin-film transistor are shown in Fig. 2(e). The measurement in air affords the electron mobility of 0.27 $cm^2 V^{-1} s^{-1}$. The value is comparable to that of **SS-Pr**. Since the thin-film transistors of **SS-EtPh** are stable under ambient conditions, the aging stability is investigated. After stored three months in air, the mobility does not change, though the threshold voltage somewhat increases. In the transistors of **SS-Pr**, an increase of the off current is observed after the storage. In contrast, the off current of the transistors of **SS-EtPh** is unchanged. It should be noted that excellent stability is realized even in the thin-film transistors.

OS-Bn shows 10^{-3} order mobility under vacuum and in the ambient atmosphere. However, the threshold voltage and off current increase in air. **OS-EtPh** shows an order of magnitude higher mobility than **OS-Bn**. Only the threshold voltage increases in air. **OS-Bn** and **OS-EtPh** show improved stability in comparison with the previously reported **OS-R**. This may be due to the introduction of the bulky substituents.[6]

Crystal structures

X-ray single crystal structure analyses were carried out for **OS-Bn**, **OS-EtPh**, **SS-Bn**, and **SS-EtPh**. The crystal data are listed in Table 3. All the molecules are situated on inversion centers. The previous **OS-R** compounds have herringbone structures,[3] but **OS-Bn** has a stacking structure (Fig. 3). The stacking structure seems to be due to the bulky benzyl groups, where the torsion angle between the core part and the phenyl ring is 105°. The molecules are uniformly stacked along the *b* axis with the interplanar distance of 3.560 Å. The adjacent columns along the *a* + *c* axis are alternately tilted in the opposite directions with respect to the molecular long axes. **OS-Bn** has the large transfer integral of 75.2 meV along the stacking direction.

SS-Bn has a stacking structure similar to **OS-Bn** (Fig. 3), but the adjacent columns are alternately tilted along the *c* axis because the space group is different from **OS-Bn**. The interplanar distance of **SS-Bn** (3.650 Å) is longer than that of **OS-Bn**, and the intrastack transfer integral (14.0 meV) is much smaller

Table 3 Crystallographic data, thin-film XRD *d* values, and the tilt angles from the substrate normal

	OS-Bn	OS-EtPh	SS-Bn	SS-EtPh
Formula	$C_{20}H_{14}N_2O_2S_4$	$C_{22}H_{18}N_2O_2S_4$	$C_{20}H_{14}N_2S_6$	$C_{22}H_{18}N_2S_6$
Formula weight	442.58	470.64	474.70	502.76
Crystal system	Monoclinic	Monoclinic	Monoclinic	Orthorhombic
Space group	$P2_1/n$	$P2_1/c$	$P2_1/c$	$Pccn$
Shape	Red needle	Orange plate	Dark purple needle	Dark purple plate
a (Å)	18.054(15)	18.891(7)	11.9840(3)	23.6666(4)
b (Å)	4.977(5)	6.409(3)	4.79313(10)	13.6498(2)
c (Å)	11.429(8)	9.138(4)	18.2901(4)	7.17290(10)
β (deg.)	108.13(4)	93.09(4)	104.4657(11)	90
V (Å^3)	976.0(14)	1104.8(8)	1017.29(4)	2317.17(6)
Z-value	2	2	2	4
T (K)	298	298	271	271
D_{calc} (g cm^{-3})	1.506	1.415	1.550	1.441
Total reflns.	3588	2475	10 789	24 371
Unique reflns. (R_{int})	2830 (0.0611)	1951 (0.1261)	1860 (0.0495)	2131 (0.0439)
R_1 [$F^2 > 2\sigma(F^2)$]	0.0548	0.0660	0.0448	0.0353
wR_2 [all reflns.]	0.1652	0.2475	0.1389	0.093
GOF	1.017	1.032	1.114	1.123
XRD *d* (Å)	10.8 (001)	19.0 (∼*a*)	15.2	18.2
Tilt angle *φ* (°)	33	24	18	50 (12)[a]

[a] The value in the thin film is in the parentheses.

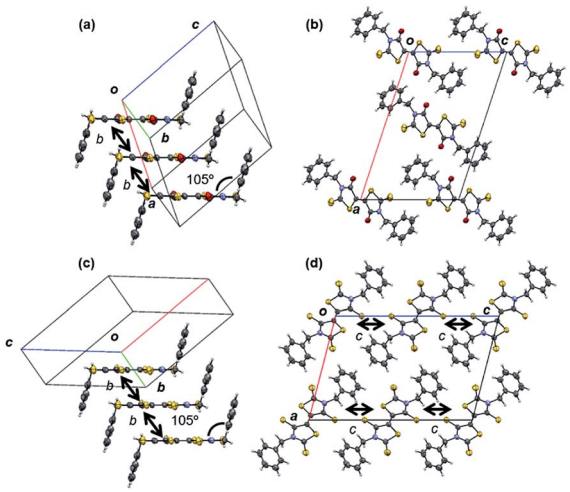

Fig. 3 Crystal structure of **OS-Bn** (a) viewed along the molecular short axis, and (b) along the *b* axis. A short intermolecular S–S distance, 3.944 Å, exists along the *b* axis. Crystal structure of **SS-Bn** (c) viewed along the molecular short axis and (d) along the *b* axis. Transfer integrals of the LUMO–LUMO interactions are $b = 14.0$ and $c = 6.2$ meV. The dihedral angel between the **OS-R** core and the phenyl ring is 105°, and the π–π stacking distance is 3.650 Å. A short intermolecular S–S distance, 3.842 Å, exists along the *b* axis.

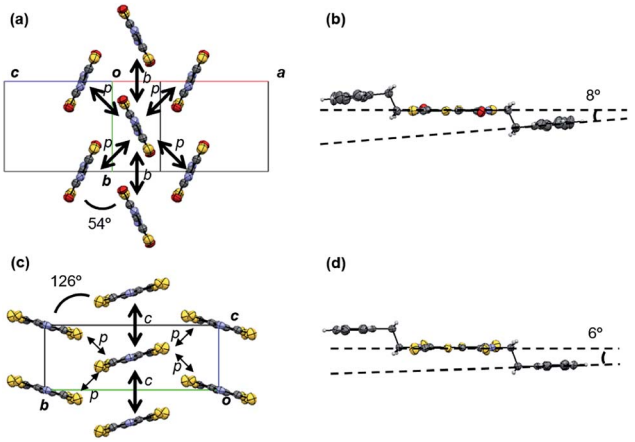

Fig. 4 (a) Crystal structure of **OS-EtPh** viewed along the molecular long axis, where the 2-phenylethyl groups are omitted for clarify. Transfer integrals of the LUMO–LUMO interactions are $b = 7.9$ and $p = 22.0$ meV. A short intermolecular S–S distance, 3.957 Å, exists along the *b* axis. (b) Molecular structure of **OS-EtPh** viewed along the molecular short axis. The dihedral angel between the core and the phenyl ring is 8°. (c) Crystal structure of **SS-EtPh** viewed along the molecular long axis, where the 2-phenylethyl groups are omitted for clarify. Transfer integrals of the LUMO–LUMO interactions are $c = -2.0$ and $p = 9.2$ meV. Short S–S distances along *p* are 3.652 and 3.666 Å. (d) Molecular structure of **SS-EtPh** viewed along the molecular short axis. The dihedral angel between the core and the phenyl ring is 6°.

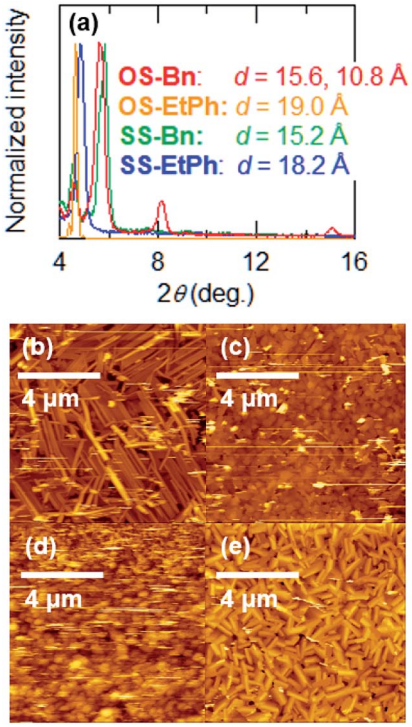

Fig. 5 (a) X-ray diffraction patterns of **XS-R**. Atomic force microscopy (AFM) images of (b) **OS-Bn**, (c) **OS-EtPh**, (d) **SS-Bn**, and (e) **SS-EtPh**.

than that of **OS-Bn**. This is in agreement with the reduced transistor performance.

OS-EtPh has a herringbone structure similar to **OS-R** (Fig. 4). Owing to the ethylene group between the core part and the phenyl ring, the torsion angle is small (8°). The small steric hindrance allows **OS-EtPh** to form the ordinary herringbone structure similar to **OS-R**. The dihedral angle is 54°, which is smallest among **OS-R**. The small dihedral angle leads to a large transfer integral (*p*) of 22.0 meV.

SS-EtPh has a herringbone structure with a large dihedral angle of 126° (Fig. 4). The structure resembles the θ-phase structure observed in bis(ethylenedithio)tetrathiafulvalene (BEDT-TTF) salts.[14] The torsion angle between the core part and the phenyl ring is as small as 6° similarly to **OS-EtPh**. The previous **SS-R** compounds have the tilted stacking structure. The large substituent inhibits the intermolecular short S–S contacts (<3.6 Å) to realize a herringbone structure. This is analogous to **OS-R**, where the weakened intermolecular interactions result in the herringbone structure.[3] CH–S interactions exist along the *p* direction (Fig. S4†), but the transfer integral (*p*) is very small.

Thin film characterizations

Thin films of the present compounds show sharp X-ray diffraction (XRD) peaks (Fig. 5(a)). The extracted *d* values are listed in Table 3. A thin film of **OS-Bn** shows an XRD peak at the *d*-spacing of 10.8 Å, which corresponds to (001) of the crystal structure. Another peak at the *d*-spacing of 15.6 Å suggests that the crystal (101) planes are parallel to the substrate, which may correspond to the molecular long axis. Although **OS-Bn** has two orientations in the thin film, the conducting columns (*b*) are parallel to the substrate in both orientations. For **OS-EtPh**, the *d*-spacing is 19.0 Å, which is almost equal to the crystallographic *a* axis. For **SS-Bn**, the *d*-spacing is 15.2 Å, and the crystal (−102) planes are likely to be parallel to the substrate, which may

correspond to the molecular long axis. For **SS-EtPh**, the *d*-spacing is 18.2 Å, but this value does not agree with any lattice constants. Since this value is lager than $a/2$, the molecules in the thin film are less tilted (12°) than those in the crystal (50°). From these results, the tilt angles (φ) of the molecular long axes from the substrate normal are estimated on the basis of $\varphi = \cos^{-1}(l/d)$ (Table 3), where l is the molecular length estimated from the crystal structure. In general, **OS-R** molecules are more largely tilted (>20°) than **SS-R** molecules (<20°). The tilt angle of **SS-EtPh** is particularly small (12°) even compared with the previously investigated **SS-R** (∼18°). Since small tilt angles are favorable in thin-film transistors,[15] this should be related to the improved transistor performance of **SS-EtPh**.

Atomic force microscopy (AFM) images of the present compounds show densely packed microcrystals (Fig. 5). In particular, **SS-EtPh** shows very good crystallinity and smooth packing. This is certainly related to the good transistor performance. **SS-Bn** shows exceptionally loose packing and poor crystallinity. This should be responsible for the absence of the transistor properties.

Conclusions

We have prepared a new series of electron-transporting organic semiconductors with bulky substituents. Irrespective of the core tetrathione and dithione structures, the benzyl groups realize a stacking structure, whereas the phenylethyl groups lead to herringbone structures. Benzyl groups have a molecular structure with large torsion angles, to construct a one-dimensional staking structure. This is, however, disadvantageous to the transistor properties. **SS-Bn** dose not show transistor behaviour even under vacuum. This is also due to the poor thin-film morphology and the small transfer integral along the stacking direction, which is five times smaller than **OS-Bn**. In **OS-Bn**, the thin-film morphology and the XRD peak indicate high crystallinity, but the transistors show considerably low mobility. This seems to come from the one-dimensional carrier transport.

OS-EtPh maintains the usual herringbone structure similar to **OS-R**. **OS-EtPh** shows the mobility of the same order of magnitude as the previous **OS-R**. Phenylalkyl groups have a great influence upon not only the crystal structure but also the stability of the transistor operation. Degradation of the mobility in the ambient conditions, which has been observed in the previous **OS-R**, is not observed in **OS-EtPh**. 2-Phenylethyl groups disturb the intermolecular S–S interactions widely observed in **SS-R**, and **SS-EtPh** forms a herringbone structure. The thin-film transistors based on **SS-EtPh** exhibit the highest mobility of 0.27 $cm^2\ V^{-1}\ s^{-1}$ among the birhodanine derivatives. Although the close intermolecular S–S contacts are largely reduced, this compound exhibits excellent stability of the transistors. The AFM image and the XRD peaks indicate high crystallinity. The *d*-spacing indicates that the molecules in the thin films are less tilted than the crystals, which is favorable to thin-film transistors.[15] This is expected to show the significant improvement of the transistor properties, because the previous **SS-R** compounds show large tilt angles (∼30°). Accordingly, introduction of bulky substituents is a versatile strategy to improve the stability of the transistor performance.

Conflicts of interest

The authors declare no competing financial interest.

Acknowledgements

This work was partly supported by ACT-C Grant Number JPMJCR12ZB from JST, Japan, and by a JPSJ KAKENHI Grant Number 16K13974. We thank the Agence Nationale de la Recherche, France (ANR project No. 12-BS07-0032) for financial support. The authors are grateful to Tokyo Institute of Technology Center for Advanced Materials Analysis for XRD measurement and Prof. Kakimoto for AFM measurements.

Notes and references

1 (*a*) Z. Zhang, J.-B. Tan, C.-P. Luo, J.-L. Xie, H.-T. Cai, L.-M. Yang, X.-P. Liu, J.-R. Zhou and C.-L. Ni, *Synth. Met.*, 2014, **195**, 147–153; (*b*) H. Moon, H. Cho, M. Kim, K. Takimiya and S. Yoo, *Adv. Mater.*, 2014, **26**, 3105–3110; (*c*) Y. Yuan, G. Giri, A. L. Ayzner, A. P. Zoombelt, S. C. B. Mannsfeld, J. Chen, D. Nordlund, M. F. Toney, J. Huang and Z. Bao, *Nat. Commun.*, 2014, **5**, 3005; (*d*) H. Iino, T. Usui and J.-I. Hanna, *Nat. Commun.*, 2015, **6**, 6828.

2 (*a*) X. Zhan, A. Facchetti, S. Barlow, T. J. Marks, M. A. Ratner, M. R. Wasielewski and S. R. Marder, *Adv. Mater.*, 2011, **23**, 268; (*b*) Y. Zhao, Y. Guo and Y. Liu, *Adv. Mater.*, 2013, **25**, 5372; (*c*) C. R. Newman, C. D. Frisbie, D. A. da Silva Filho, J.-L. Brédas, P. C. Ewbank and K. R. Mann, *Chem. Mater.*, 2004, **16**, 4436; (*d*) X. Gao and Y. Hu, *J. Mater. Chem. C*, 2014, **2**, 3099; X. Gao, C. Di, Y. Hu, X. Yang, H. Fan, F. Zhang, Y. Li, H. Li and D. Zhu, *J. Am. Chem. Soc.*, 2010, **132**, 3697. (*e*) Y. Hu, X. Gao, C. Di, X. Yang, F. Zhang, Y. Liu, H. Li and D. Zhu, *Chem. Mater.*, 2011, **23**, 1204; (*f*) Y. Hu, Z. Wang, X. Zhang, X. Yang, C. Ge, L. Fu and X. Gao, *Org. Lett.*, 2017, **19**, 468; (*g*) L. Tan, Y. Guo, Y. Yang, G. Zhang, D. Zhang, G. Yu, W. Xu and Y. Liu, *Chem. Sci.*, 2012, **3**, 2530; (*h*) J. T. E. Quinn, J. Zhu, X. Li, J. Wang and Y. Li, *J. Mater. Chem. C*, 2017, **5**, 8654; (*i*) J. Dhar, U. Salzner and S. Patil, *J. Mater. Chem. C*, 2017, **5**, 7404.

3 A. Filatre-Furcate, T. Higashino, D. Lorcy and T. Mori, *J. Mater. Chem. C*, 2015, **3**, 3569.

4 K. Iijima, Y. Le Gal, T. Higashino, D. Lorcy and T. Mori, *J. Mater. Chem. C*, 2017, **5**, 9121.

5 F. Nasiri, A. Zolati and S. Asadbegi, *J. Heterocyclic Chem.*, 2016, **53**, 989.

6 (*a*) H. Minemawari, M. Tanaka, S. Tsuzuki, S. Inoue, T. Yamada, R. Kumai, Y. Shimoi and T. Hasegawa, *Chem. Mater.*, 2017, **29**, 1245; (*b*) K. Takimiya, S. Shinamura, I. Osaka and E. Miyazaki, *Adv. Mater.*, 2011, **23**, 4347.

7 O. Pitayatanakul, T. Higashino, M. Tanaka, H. Kojima, M. Ashizawa, T. Kawamoto, H. Matsumoto, K. Ishikawa and T. Mori, *J. Mater. Chem. C*, 2014, **2**, 9311.

8 D. Yoo, T. Hasegawa, M. Ashizawa, T. Kawamoto, H. Masunaga, T. Hikima, H. Matsumoto and T. Mori, *J. Mater. Chem. C*, 2017, **5**, 2509.

9 (*a*) M. Kanno, Y. Bando, T. Shirahata, J. Inoue, H. Wada and T. Mori, *J. Mater. Chem.*, 2009, **19**, 6548; (*b*) J. Nagakubo, M. Ashizawa, T. Kawamoto, A. Tanioka and T. Mori, *Phys. Chem. Chem. Phys.*, 2011, **13**, 14370.

10 (*a*) C. Roussel, R. Gallo, M. Chanon and J. Metzger, *Bull. Soc. Chim. Fr.*, 1971, **5**, 1902; (*b*) Y. Le Gal, N. Bellec, F. Barrière, R. Clérac, M. Fourmigué, V. Dorcet, T. Roisnel and D. Lorcy, *Dalton Trans.*, 2013, **42**, 16672; (*c*) Y. Le Gal, D. Ameline, N. Bellec, A. Vacher, T. Roisnel, V. Dorcet, O. Jeannin and D. Lorcy, *Org. Biomol. Chem.*, 2015, **15**, 8479.

11 M. L. Tang, A. D. Reicharrdt, P. Wei and Z. Bao, *J. Am. Chem. Soc.*, 2009, **131**, 5264.

12 H. Usta, A. Facchetti and T. J. Marks, *Acc. Chem. Res.*, 2011, **44**, 501.

13 (*a*) M. Kraus, S. Richler, A. Opitz, W. Brütting, S. Haas, T. Hasegawa, A. Hinderhofer and F. Schreiber, *J. Appl. Phys.*, 2010, **107**, 094503; (*b*) M. Kraus, S. Haug, W. Brütting and A. Opitz, *Org. Electron.*, 2011, **12**, 731.

14 (*a*) H. Mori, S. Tanaka, T. Mori, A. Kobayashi and H. Kobayashi, *Bull. Chem. Soc. Jpn.*, 1998, **71**, 797; (*b*) H. Mori, S. Tanaka and T. Mori, *Phys. Rev. B: Condens. Matter Mater. Phys.*, 1998, **57**, 12023.

15 (*a*) T. Kakinuma, H. Kojima, M. Ashizawa, H. Matsumoto and T. Mori, *J. Mater. Chem. C*, 2013, **1**, 5395; (*b*) O. Pitayatanakul, K. Iijima, M. Ashizawa, T. Kawamoto, H. Matsumoto and T. Mori, *J. Mater. Chem. C*, 2015, **3**, 8612.